Multi-stable Miura-ori structures

Alessio Gorgeri[1,2]
alessio.gorgeri@polimi.it

[1]Department of Aerospace Science and Technology, Politecnico di Milano
Via La Masa 34, 20156 Milan, Italy
[2] Graduate Aerospace Laboratories (GALCIT), California Institute of Technology
1200 E California Blvd. MC 105-50, Pasadena, CA 91125

October 2018

Abstract

Mass and volume restrictions are always strict requirements for space applications. To cope with launch-vehicles size limitations, large structures - antennas, solar arrays, telescopes to say some - are traditionally assembled in space, requiring a huge amount of resources and posing complex technological challenges.
Newborn structures are designed according to this major constraint so that they can be packaged for launch and deployed once in space. Early designs included joints, hinges, actuators resulting in severe mass inefficiencies. The answer could be found in origami-like structures that integrate all the aforementioned components in a compact and reliable manner.
Miura-origami structures are plates or shells that can be folded to drastically reduce their size; these structures are often characterized by simple units that are repeated several times. Early application has regarded collapsible solar panels pioneering mounted onto the Japan's Space Flyer Unit.
The ambitious goal of current researches at Caltech is to pave the way towards the realization of reconfigurable antennas and telescopes based on multi-stable structures. The key idea is to substitute the classical folds of a Miura ori structure (that are equivalent to perfect hinges) with torsional springs. The resulting structure can exhibit multistability, a condition for which several local minima of the potential energy exist. Actuators are needed purely to morph from one to an adjacent target configuration, therefore no power is required for most of the operational life.
The present work, early stage of the ambitious project, deals with the mechanical characterization of integrated hinges. Such hinges can be realized by laser-cutting a specific pattern from flat plates, creating a weaker region along which the structure can bend. The maximum allowed rotation is far higher than that of the original material as the deformation is distributed along several strips.
The study involves several steps: first, the raw material is characterized in terms of shear and tensile stiffness; second, analytical models are developed and experimental tests are performed to study the mechanical response of simple strips - the basic blocks of the aforementioned hinges; third, the combination of analytical, numerical and experimental approaches is adopted for such hinges, trying to match the results. Several problems emerged throughout the work such as inconsistencies of the analytical models in dealing with additional phenomena such as visco-elasticity and spurious deformation patterns. While important results have been demonstrated, many additional obstacles have to be overcome as part of future works.
Keywords: Multi-stable structures, composites, analytical, numerical, experimental

1. Introduction

This introductory sections provides some basic information that are then used throughout the work.

Kinematic models are first presented as the way a 3D elastic problem is converted into simpler 2D problems; plates - structures for which one dimension (thickness) is significantly smaller than the others - are suitable targets for this approach.

Some basic concepts about Miura origami are also presented, underlining the general framework in which the present work is placed.

Sections 2 to 6 shows some of the activities that have been carried out, presented in logical and chronological order. Section 7 summarizes the obtained achievements and provides some information regarding the next steps to be taken.

1.1. Kinematic models

It will be shown that most of the problems that are presented deal with flat plates; it is therefore im-

portant to present the kinematic assumptions that allow to build a simplified 2D model of the 3D continuum. Kirchhoff-Love theory is chosen, meaning that the displacement components are expressed as:

$$\begin{aligned} u(x,y,z) &= u_0(x,y) - zw(x,y)_{/x} \\ v(x,y,z) &= v_0(x,y) - zw(x,y)_{/y} \\ w(x,y,z) &= w_0(x,y) \end{aligned} \tag{1}$$

where (x, y) map the reference surface and z maps the thickness directions, u and v are the in-plane displacement components, z is the out of plane displacement component. Quantities marked with the subscript "0" refer to the reference surface (for example $u_0(x, y)$ is the displacement component along the x direction of points belonging to the reference surface) while the notation $q_{/r}$ denotes the derivative of a generic quantity q with respect to the variable r (where $r = x, y, z$).

Through the gradient equations, the in-plane components of the strain field are

$$\begin{aligned} \varepsilon_x &= u_{/x} = u_{0/x} - zw_{/xx} \\ \varepsilon_y &= v_{/y} = v_{0/y} - zw_{/yy} \\ \gamma_{xy} &= u_{/y} + v_{/x} = u_{0/y} + v_{0/x} - 2zw_{/xy} \end{aligned} \tag{2}$$

while the out-of-plane strain components identically equals zero

$$\begin{aligned} \gamma_{yz} &= v_{/z} + w_{/y} = 0 \\ \gamma_{xz} &= u_{/z} + w_{/x} = 0 \\ \varepsilon_z &= w_{/z} = 0 \end{aligned} \tag{3}$$

The strain vector is compactly written as

$$\boldsymbol{\varepsilon} = \boldsymbol{\varepsilon}_0 + z\mathbf{k} \tag{4}$$

where

$$\boldsymbol{\varepsilon}_0 = \begin{Bmatrix} u_{0/x} \\ v_{0/y} \\ u_{0/y} + v_{0/x} \end{Bmatrix} \quad , \quad \mathbf{k} = \begin{Bmatrix} w_{/xx} \\ w_{/yy} \\ 2w_{/xy} \end{Bmatrix} \tag{5}$$

For composites, ply specific constitutive relations are expressed as

$$\begin{Bmatrix} \sigma_x \\ \sigma_y \\ \tau_{xy} \end{Bmatrix} = \begin{bmatrix} \tilde{Q}^k_{11} & \tilde{Q}^k_{12} & \tilde{Q}^k_{16} \\ \tilde{Q}^k_{12} & \tilde{Q}^k_{22} & \tilde{Q}^k_{26} \\ \tilde{Q}^k_{16} & \tilde{Q}^k_{26} & \tilde{Q}^k_{66} \end{bmatrix} \begin{Bmatrix} \varepsilon_x \\ \varepsilon_y \\ \gamma_{xy} \end{Bmatrix} \tag{6}$$

The along the thickness integral of the stress components leads to the well known

$$\begin{Bmatrix} N \\ M \end{Bmatrix} = \begin{bmatrix} \mathbf{A} & \mathbf{B} \\ \mathbf{B} & \mathbf{D} \end{bmatrix} \begin{Bmatrix} \boldsymbol{\varepsilon}_0 \\ \mathbf{k} \end{Bmatrix} \tag{7}$$

where additional details can be found in [1].

For symmetric laminates (which is always the case) the equivalent Young's modulus along the x direction is computed as

$$E_1 = \frac{1}{S_{11}} \tag{8}$$

where $\mathbf{S} = \mathbf{A}^{-1}$. Similarly, the in-plane shear modulus is

$$G_{12} = \frac{1}{S_{66}} \tag{9}$$

Equations (7), (8) and (9) will be used in the following.

1.2. Miura origami

When talking about Miura ori (or Miura fold, where the name comes from its Japanese inventor, Koryo Miura) we refer to techniques used to collapse a flat structure into a smaller area. The basic idea is to fold the structure along a very specific and repeated pattern, see for example [2, 3] and Figure 1, from Wikipedia.

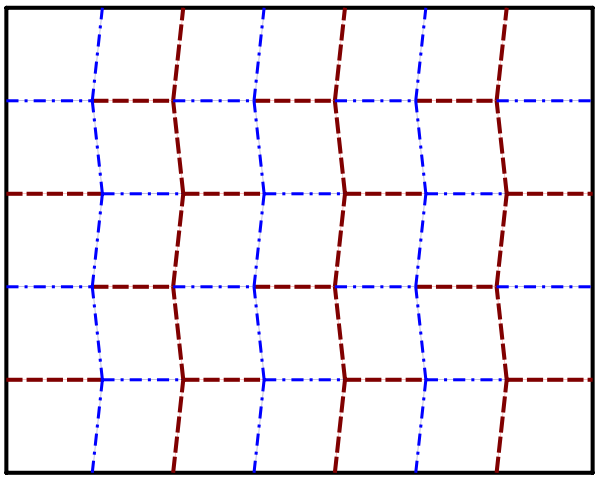

Figure 1: Crease pattern for a Miura fold. The parallelograms of this example have 84° and 96° angles.

Throughout the last decades the Miura ori technique has attracted much interest for designing collapsible and deployable structures, allowing for instance to obtain large solar arrays that could be packaged during the launch phase to cope with the strict payload volume limitations.

Within this context, Yang Li[1] is working on a new design of re-configurable antennas and mirrors that can morph with reduced effort and achieve high shape accuracy.

The idea is to have a set of flat plates connected at the edges by hinges that constrain the relative motions except for the mutual rotation along the common edge. A small set of such plates is repeated several times to obtain large structures; these structures are characterized by several degrees of freedom that in turn identify all the possibly configurations they can assume (∞^n where n is the number of internal degrees of freedom).

If the hinges are substituted with torsional springs, each characterized by its own rest angle and

[1] Yang Li, Post Doctoral researcher, Graduate Aerospace Laboratories (GALCIT), California Institute of Technology, 1200 E California Blvd. MC 105-50, Pasadena, CA 91125

torsional stiffness, a potential energy is then associated with the manifold of kinematically allowed configurations. By means of a smartly designed algorithm it is then possible to pick some desired configurations and adjust the springs parameters such that the potential energy will have local minima in correspondence to the target configurations; the additional design freedom is used to have sharp and deep minima to boost the shape accuracy. A small set of actuators is then required to jump between adjacent configurations, while no power is required to maintain such configurations.

Prototypes were developed that confirmed the potentiality of the method, but resulted in being rather heavy and complex.

A breakthrough idea was to integrate the torsional springs in the flat plates, therefore reducing weight, complexity and, on a further extent, costs. Such integrated springs can be realized thanks to the laser-cut techniques, as will be shown in the following.

2. Material characterization

As already outlined, it is possible to identify a small unit that is repeated several times in the Miura origami multistable structure that has to be designed. Each unit is in turn characterized by a certain number of fold regions that can be modelled as rotational springs with a certain stiffness that depends on the topology of the laser-cut.

Previous studies were focused on the realization of one of such hinges in order to check the prediction accuracy of available analytically models; samples were built from steel plates, laser-cutting a specific pattern as shown in Figure 2.

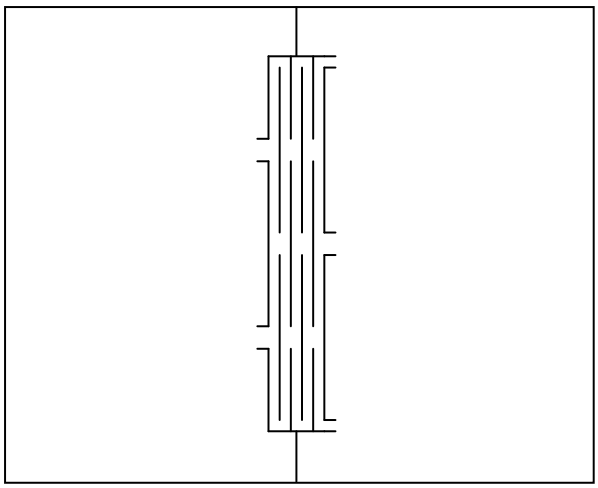

Figure 2: Drawing used to create an integrated hinge in a flat plate.

The main advantages of steel plates is that the mechanical response is accurately described by simple relations (i.e. linear hyperelastic behaviour); as a results, the experimental data accurately matched the numerical ones.

Relevant improvements in terms of stiffness to weight ratio and mitigation of electromagnetic interference could be achieved by using composite materials, provided complex the mechanical response can be accurately predicted. As previously outlined, this is the main focus of the research.

As for preliminary studies, cheap and readily available plates made by glass fibres / epoxy resin were chosen; in addition, such combination is characterized by a relatively wide elastic range (in terms of maximum elastic strain) and does not interfere with electromagnetic fields. The main issue is that no information were provided in terms of elastic coefficients, stacking sequence, fibres orientation.

Micrographs revealed that the plates were made by several plain weave laminae with fixed orientation, therefore an analytical model could be easily developed.

Tensile and shear tests were performed to determine the unknown elastic coefficients by fitting the analytical expression to the numerical results.

2.1. Tensile tests

Equivalent Young's modulus along several in-plane directions can be obtained by means of a tensile test. Dogbone-shaped samples are cut from the aforementioned plates as shown in Figure 3.

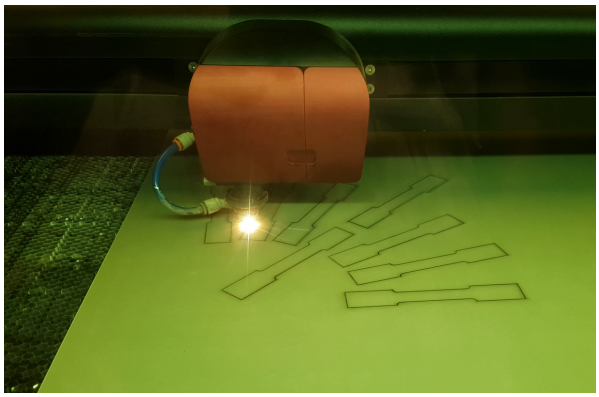

Figure 3: Laser-cut is used to manufacture glass/epoxy dogbones for tensile tests.

The test is performed using a standard Instron apparatus as shown in Figure 4. High measurement accuracy is guaranteed by means of a laser monitoring the distance between two reflective strips initially placed on the central part of the sample.

The equivalent Young's modulus along several directions is the angular coefficient of the strain-stress ($\sigma - \varepsilon$) curve, namely

$$E = \frac{\sigma}{\varepsilon} \tag{10}$$

where $\sigma = N/A$, N is the axial force that is directly measured by the instrument (through a load cell), $A = 15 \times 0.79$ mm^2 is the cross-section area and $\varepsilon =$

Figure 4: The Instron apparatus is used for tensile tests. The strain is monitored by a laser.

$(d - d_0)/d_0$, d is the distance between the reflective strips as measured by the laser and d_0 is the initial value of such distance (corresponding to a null value of the axial force).

Figure 5 shows the experimental data and the curve that minimizes the error when fitting those data, corresponding to the following elastic coefficients in the orthotropic frame

$$E_1 = E_2 = 26 \text{ GPa}$$
$$G_{12} = 5.2 \text{ GPa}$$
$$\nu_{12} = 0.136$$

It should be observed that the experimental data predict slightly different elastic moduli for the "0" and "90" directions (warp and weft directions are not equivalent). The choice is in stead to assume them equal in order to simplify the model, without giving away much accuracy.

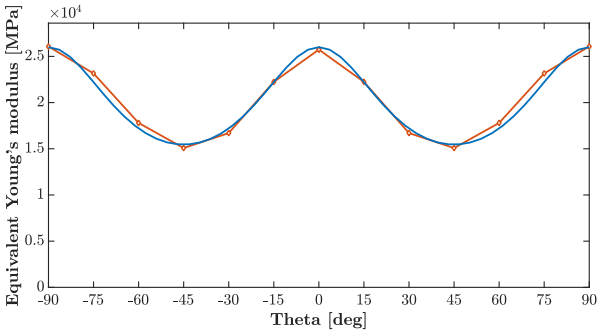

Figure 5: The experimental data (red points) are best-fit (blue curve) to determine the unknown elastic coefficients.

2.2. Shear tests

Shear tests were conducted to verify the prediction accuracy of the model for what concerns shear moduli along different directions. The setup is shown in Figure 6, where the central portion of a rectangular plate is forced to slide downwards, shear-deforming the two strips confined between the supports. Vertical displacements d is measured with lasers to ensure high accuracy measurements; force T is directly recorded by the instruments.

Figure 6: The Instron apparatus is used for shear tests. The displacement is monitored by a laser while the central strip is pushed downwards.

Say that each strip has height l, width w and thickness t, the shear stress τ and engineering shear strain γ are, respectively

$$\tau = \frac{T}{2ht} \qquad \gamma = \frac{d}{w} \tag{11}$$

therefore the shear modulus is computed as

$$G = \frac{\tau}{\gamma} = \frac{Tw}{2htd} \tag{12}$$

The experimental results are compared against the analytical model, as shown in Figure 7. Good agreement is obtained, therefore bending and torsion response can be eventually predicted.

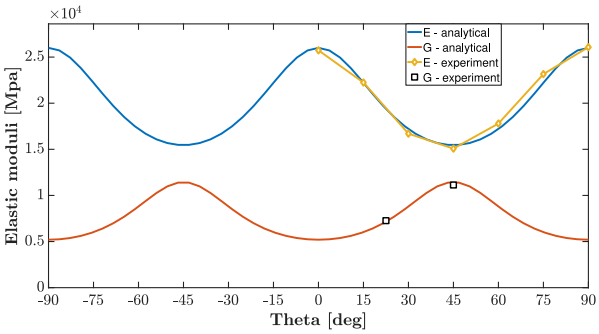

Figure 7: The experimentally obtained shear moduli (black bordered squares) are compared with the analytical model (red curve)..

3. Strips mechanical response

Before moving to the full hinge, an intermediate step is required, which is testing simple strips in torsion and bending. It will be shown that, depending on the chosen design, two types of hinges exist for which the response is bending or torsion dominated.

3.1. Bending of rectangular strips

A first attempt to model the bending response is done neglecting the torsion-bending coupling influence on bending stiffness K_b, therefore, once the Young's modulus E along the strip direction is determined, the stiffness is computed as

$$K_b = \frac{EI}{l} \tag{13}$$

where $l = 8$ cm is the strip length, $I = wt^3/12$ is the cross-section inertia with strip width $w = 3$ cm and thickness $t = 0.794$ mm. Strips were cut along the 0, 45, 90 direction and tested, measuring the slope of the bending-rotation curve (the experimental setup is described in Subsection 4.2).

Table 1: Bendind stiffness expressed in Nmm/rad for rectangular strips cut along 0, 45 and 90 directions.

	[0/90]	[+45/-45]	[90/0]
Experimental	380.6	398.5	239.1
Theoretical	405.4	405.4	241.0
Error	6.5%	1.7%	0.5%

Results reported in Table 1 show that the bending response can be predicted with high accuracy, therefore it was possible to immediately test different loading conditions.

3.2. Torsion of rectangular strips

The torsion response of rectangular strips is analytically modelled according to two different theories that yield similar results. Strips can be in fact seen as narrow flat plates or composite beams with rectangular cross-section, as shown in the following.

Plate twisting According to the Kirchhoff-Love kinematic description, a plate with length, width, thickness ($l \times w \times t$), simply supported at two opposite corners and loaded by P/2 at the others deforms in such a way that the free corners move downwards by a quantity δ that is related to P [4]

$$\frac{\delta}{P} = \frac{lw}{16 D_{66}} \tag{14}$$

where, according to the chosen kinematic model, the twisting stiffness is

$$D_{66} = \frac{1}{3} \sum_{k=1}^{N_k} \tilde{Q}_{66}^k \left(z_k^3 - z_{k-1}^3 \right) \tag{15}$$

The equivalent torque and rotation are simply computed as, respectively

$$T = \frac{Pw}{2} \qquad \phi = \frac{2\delta}{w} \tag{16}$$

therefore the torsion stiffness is

$$\frac{T}{\phi} = \frac{4 D_{66} w}{l} \tag{17}$$

Bar torsion Under certain hypotheses, the geometric torsional rigidity of a bar with rectangular cross-section area (width w and thickness t) can be computed according to the Roark's formula [5]

$$K = wt^3 \left[\frac{1}{3} - 0.21 \frac{t}{w} \left(1 - \frac{t^4}{12 w^4} \right) \right] \tag{18}$$

The torsional stiffness is easily computed as

$$\frac{T}{\phi} = \frac{KG}{l} \tag{19}$$

where G is the (proper) in-plane shear modulus.

Experimental results Similarly to what previously assessed for the bending case, experimental tests are conducted to check the prediction accuracy of the model(s).

The test setup is shown in Figure 8. The right-end is manually rotated with high accuracy (about 3/100°), whilst the resulting torque is measured at the opposite end with a Force/Torque transducer (ATI's F/T Sensor: Nano17, calibration SI-12-0.12, sensitivity 1/64 Nmm); a slider is adopted to keep the axial movements unconstrained.

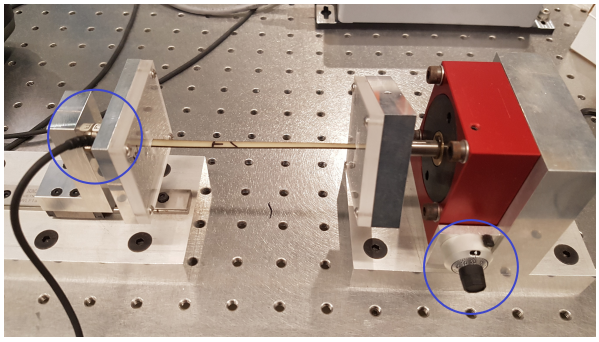

Figure 8: Torsion set-up.

Contrarily to what happens for the bending case, where the experimental data accurately match the analytical predictions, unacceptable discrepancies are observed, as shown in the following.

Several different strips are tested in order to correlate the error to some geometrical features (either length or width *per se* or a proper combination of those); the samples are 0.794 mm thick and their in plane dimensions ($w \times l$) are, in order:

1. (5×100) mm^2
2. (10×150) mm^2
3. (15×150) mm^2
4. (15×75) mm^2
5. (30×150) mm^2

The torsional rigidity is the slope of the (experimentally obtained) torque-rotation curve, and is compared with analytical data, according to the bar and plate models. Results are presented in Table 2. A clear trend is observed, which is, the analytical models predict lower stiffness as the width increases, independently from the strip length. This can be explained observing that the displacement field close to the constrained edge does not resemble a pure torsion, as clearly observed in Figure 9; seemingly, this effect is more severe as the strip width increases.

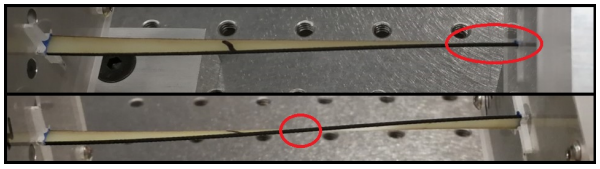

Figure 9: End-effect. The strip looks stiffer.

Additional attempts to explain the inconsistency of the results were also performed. To mention one, corrected formulas for bar torsion to better account for the anisotropicity (see for example [6] and [7]) can be used. The corrected torsional rigidity is

$$\frac{T}{\phi} = G_{xy}\frac{wt^3}{L}\beta \tag{20}$$

where β is given by

$$\beta = \frac{32a^2G_{yz}}{\pi^4 b^2 G_{xy}} \sum_{n=1,3,5,}^{\infty} \frac{1}{n^4} \cdots \\ \cdots \left[1 - \frac{2a}{n\pi b}\sqrt{\frac{G_{yz}}{G_{xy}}}\tanh\left(\frac{n\pi b}{2a}\sqrt{\frac{G_{xy}}{G_{yz}}}\right)\right] \tag{21}$$

For the material in use however, this correction (which is driven by the magnitude of in-plane to out-of-plane shear moduli ratio) is of about few percent, therefore does not explain the observed differences in toto.

Additional attempts to model the exact response are shown in Section 5.

4. Hinges mechanical response

As previously observed, the characterization of torsion and bending response of rectangular strips is the first step in designing hinges that are in turn the basic blocks of Miura-ori structures.

In order to obtain hinges that can undergo large rotations (of more than 90 degrees) without hitting the plastic regime, very specific patterns should be cut from the glass fibre/epoxy plates, see for example [8].

The driving idea is to have long load paths in such a way that small deformations can still produce large overall rotations, as already shown in Figure 2. That design however, was considered obsolete because of the resulting unacceptable twisting compliance, therefore improved geometries were manufactured.

4.1. Torsion dominated behaviour

Small but relevant improvements led to a new design, which is shown in Figure 10 (note that the circular holes are needed to interface the testing apparatus and have no other use).

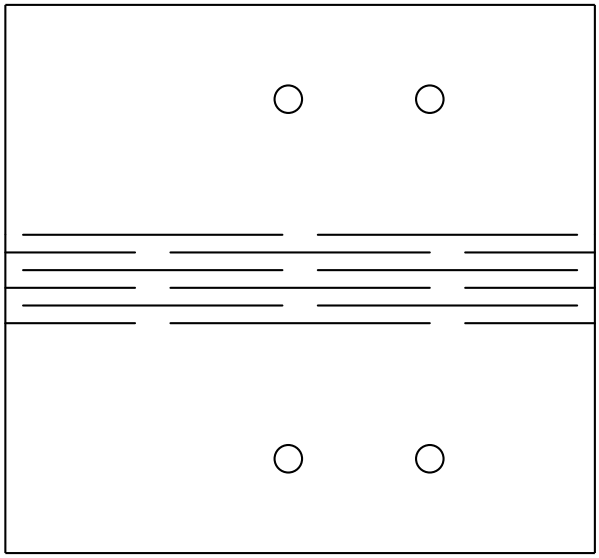

Figure 10: A hinge designed to be torsion dominated.

When the plate is bent, the long transverse strips undergo torsion, reason why the hinge behaviour is referred to as "torsion dominated". Torsion is transmitted from one to the following strip through short (i.e. strong) sections that deform in bending. A first approximation is made by neglecting the bending compliance; therefore, referring to Figure 10, the elastic response is represented by a 4-elements parallel of 5-elements series of torsional springs. As it turns out, the bending stiffness of the hinge is:

$$K_b^{hinge} = \frac{4}{5}K_t \tag{22}$$

Samples are cut along the 0 and 45 directions, and the bending stiffness is experimentally tested (the set-up is shown in Subsection 4.2).

Table 2: Torsional stiffness expressed in Nmm/rad for a set of strips numbered from 1 to 5, cut along the 0 and 45 directions.

	[0/90]					[+45/-45]				
	1	2	3	4	5	1	2	3	4	5
Experimental	36.32	62.91	110.8	225.6	265.3	73.46	128.2	217.0	429.2	459.5
Bar theory	39.04	54.95	83.87	167.7	170.6	85.89	120.9	184.5	369.0	375.4
Error (%)	+7.5	−13	−24	−26	−36	+16	−5.7	−15	−14	−18
Plate theory	43.40	57.87	86.80	173.6	173.6	85.00	113.3	170.0	340.0	340.0
Error (%)	+20	-8.0	-22	−23	−35	+15	−12	−22	−21	−26

The results are shown in Table 3, compared to the theoretical predictions using the proposed models.

Table 3: Bendind stiffness expressed in Nmm/rad for a torsion dominated hinge.

	[0/90]	[+45/-45]
Experimental	102	168
Theoretical	134	295
Error	31%	75%

It is clear that the obtained errors are not acceptable, therefore some improvements were necessary.

A clear hint comes from the fact that the hinge is always softer than what predicted, therefore the torsion is not transmitted with zero compliance from one strip to the other. In addition, this effect is more severe when the strips are torsion strong (45 degrees), in which case the connections are necessarily bending weak.

Despite the big errors, it was still possible to draw some conclusions. In order to address the problem, several options were available; on top of that, the choice to completely redesign the hinge, so that the behaviour would be bending dominated (therefore predictable with higher confidence).

4.2. Bending dominated behaviour

After a topology optimization procedure (remember that the hinge has to allow large rotations without hitting the plastic regime while being compact to enable sharp bending - requirements that conflict each other) a new design is proposed in Figure 11.

In contrast with the previous one, the mechanical response is "bending dominated"; bending is transferred from one strip to the following through a short (i.e. strong) section that deforms in torsion. The mechanical response is therefore modelled as a 2-elements parallel of 5-elements series of bending springs. As it turns out, the bending stiffness of the hinge is:

$$K_b^{hinge} = \frac{2}{5} K_b \tag{23}$$

Samples are cut along the 0 and 45 directions, and the bending stiffness is experimentally tested. Figure 12 shows the set-up.

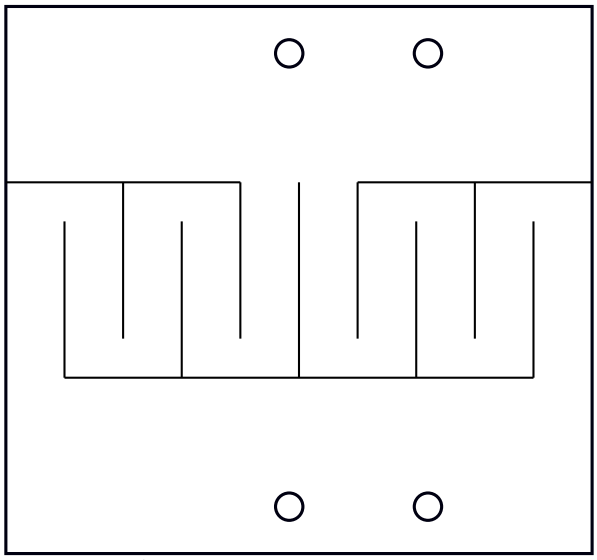

Figure 11: A hinge designed to be bending dominated to address some issues related with torsion.

A plate is clamped (by means of the previously shown holes) to supports that are free to slide longitudinally. The two ends can be manually rotated (blue circles) with high accuracy of about 2.3/100°; extensometers are placed on both shafts while the strain is read via a digital display (red circle). The test procedure is rather time-consuming, in fact, the user has to manually rotate the shafts until the two strain values match exactly to ensure that pure bending condition is achieved.

The results are shown in Table 4, compared to the theoretical predictions.

Table 4: Bendind stiffness expressed in Nmm/rad for a bending dominated hinge.

	[0/90]	[+45/-45]
Experimental	134	96.6
Theoretical	163	96.7
Error	22%	0.1%

The obtained results are of great importance. First, the experimentally obtained stiffness is never higher then what is predicted by the model, which is reasonable since we are neglecting the compliance of the transition regions. Second, when the hinge is "bending weak" the results are in perfect agree-

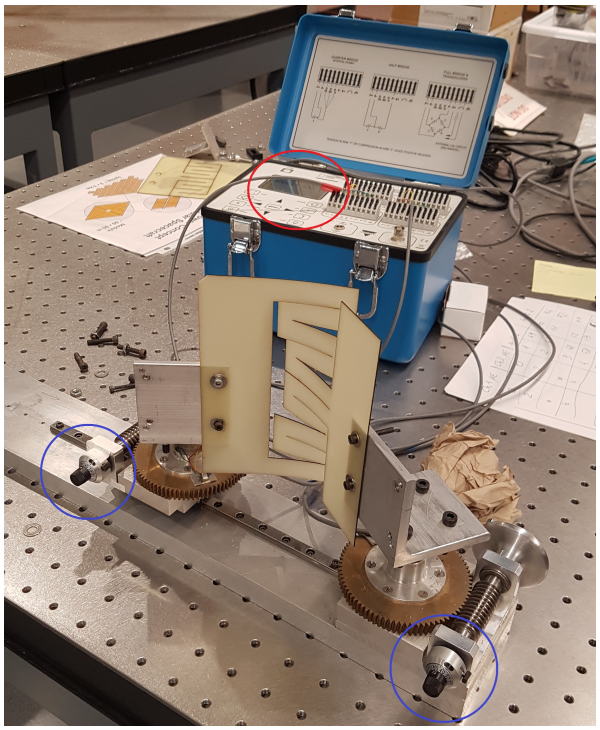

Figure 12: Bending set-up. Both movements and readings are manual. The strain of the shafts is used to measure the applied torque

ment because the transition regions are "torsion stiff" and provide effectively no compliance. On the other hand, when the hinge is "bending stiff", the transition regions are more compliant and their contribution is non-negligible.

This intuition is confirmed when closely observing the deformation pattern, as shown in Figure 13.

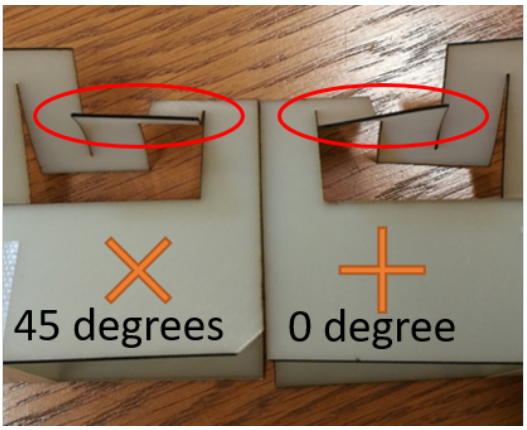

Figure 13: Additional compliance when the connections are weaker than the main strips. The displacement field for the [+45/-45] is extremely regular.

It is evident that the [+45/-45] hinge performs as expected while additional twisting is present for the other sample. Modelling this behaviour is a hard task, in fact, twisting/bending coupling is not strictly confined to the connection regions.

5. Additional models

Additional strategies to tackle the presented problems were explored, some of which are reported in the following.

5.1. Finite Element Model

Observing that in most of the cases the displacement field does not resemble a pure torsion (bending), a finite element model was developed (Abaqus Explicit) to get some additional insight. A mutual rotation is imposed to the rigid plates connected through the hinge while the resulting bending moment is computed; the deformed model is shown in Figure 14 while the comparison of theoretical, numerical and experimental results is in Table 5.

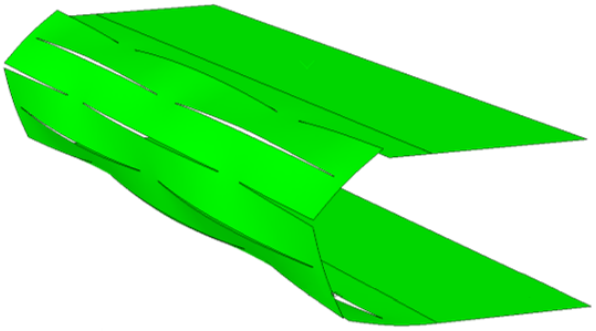

Figure 14: FEM model of the bending dominated hinge.

Table 5: Bending stiffness expressed in Nmm/rad for a torsion dominated hinge; comparison between experimental, theoretical and numerical values.

	[0/90]	[+45/-45]
Experimental	102	168
Theoretical	134 (31%)	295 (75%)
Numerical	109 (6.9%)	174 (3.6%)

Close agreement is found between numerical and experimental results. The accurate analysis of the deformation pattern obtained through fem models could therefore be the starting point to develop accurate analytical model.

5.2. Manual layup

Attempts to reduce the compliance of the transition regions were performed. Out of the many solution strategies, a very interesting option was to manufacture the flat plates in such a way to obtain a quasi-isotropic structure. It was believed that having a fibres dominated behaviour along all directions could even out the inconsistencies.

Pre-preg layers of plain weave glass fibre/epoxy are stack according to the scheme $[0/45]_{5s}$, the laminate is then insertend in a vacuum bag (Figure 15) and cured in autoclave.

The experimental campaign involving hinges made by this new material has yet to start, still it

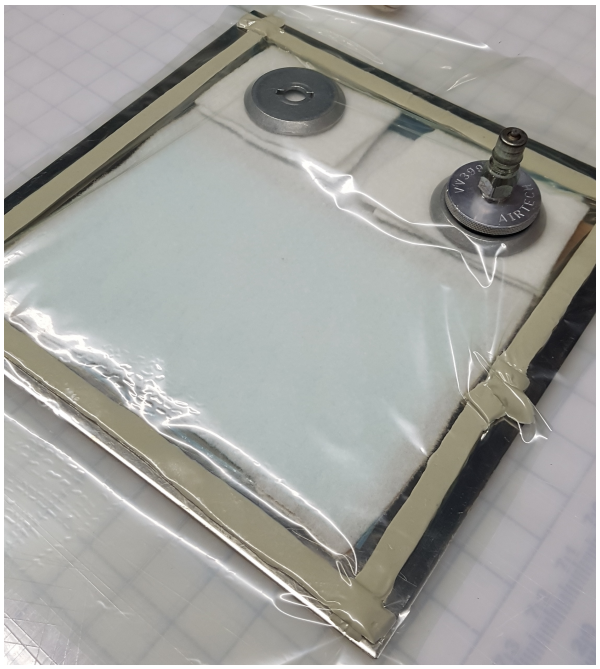

Figure 15: A composite plate is self manufactured to achieve a quasi-isotropic response - less sensitive to visco-elastic phenomena. The plate is sealed in a vacuum bag and cured in autoclave.

was possible to test some strips for a different phenomenon that was observed, which is relaxation or viscoelasticity, as described in Section 6.

5.3. Iterative design

A completely different approach to tackle the presented issue - which indeed is adopted by many research groups dealing with similar problems - is to rely on a so called iterative design.

The driving idea is that it is trivial to understand whether increasing (or decreasing) a specific geometrical feature will increase or decrease the hinge bending stiffness.

Say for example that a hinge is first designed according to the available analytical models; if the resulting stiffness (experimentally tested) is lower than expected, the second iteration should ensure a load path with a higher width-to-length ratio. A couple iterations are needed at most to obtain the desired accuracy; in addition, a database can be created collecting all the results, possibly containing information useful for future designs.

6. Relaxation

It was not mentioned before that due to the nature of the chosen material it is likely that the visco-elastic behaviour plays an important role. Relaxation phenomena are very dangerous for the target application: after the structure will be kept folded for a certain amount of time (in the order of days or weeks) it is possible that it will lose the ability to morph with desired accuracy (or at all).

As a preliminary test, samples were constrained in the deformed shape for a certain amount of time (usually 12-24 hours, see Figure 16) to get a first insight into the problem.

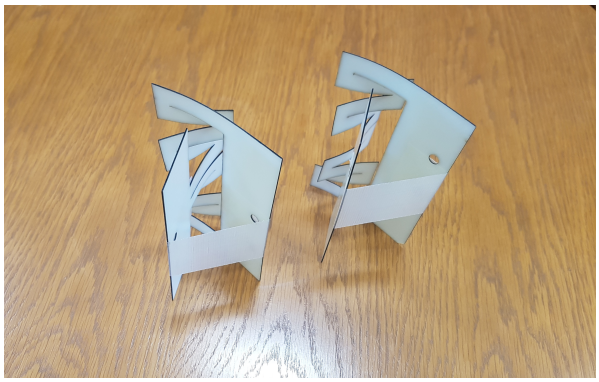

Figure 16: Samples are keps folded overnight to get a first insight of relaxation phenomena.

Not surprisingly, after the constrain was removed, the samples showed a residual deformation due to visco-elastic (relaxation) phenomena. Taking a closer look it was clear that the effect was more severe where the principal directions of the stress field were not aligned with the fibres.

It was obvious that this issue had to be studied and addressed, which is an other reason for attempting to realize a quasi-isotropic plate, as shown in Subsection 5.2.

Two options were considered, namely (i) solve the problem from the material point of view, lowering the relaxation down to a level where it can be neglected, or (ii) develop a modified design scheme in which the relaxation (whether accurately predicted) could be considered.

Tests were performed in order to quantify the relaxation at ambient temperature. Rectangular strips made of the two described materials were used. The strips were torsioned (using the very same set-up) to a comparable strain level, safely below the plastic regime; samples were kept for 14 hours while constantly monitoring the applied torque.

Figure 17 shows the experimental results. The numbers - 1 and 2 - refer to the material being the commercial or self manufactured glass fibre / epoxy composite; note that weak and strong refer to the directions along which the strip is cut from the plate to obtain the maximum or minimum torsion stiffness.

It was said that one of the purposes of the newly designed laminate was to have fibres dominating the response in about all directions, therefore increasing the stiffness and reducing the impact of relaxation. While this guess was experimentally confirmed, it should be noticed that the stronger direction gets more sensitive to visco-elastic phenomena, therefore

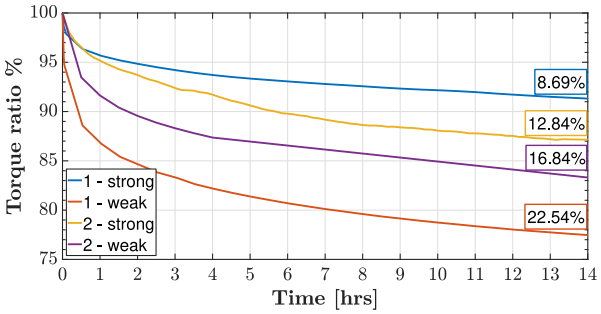

Figure 17: Relaxation effect on different samples. The behaviour of material 2 is more uniform along the strongest and weakest directions than material 1.

a trade-off should be sought.

The experimental campaign, although much time consuming, is still ongoing as it is believed to output precious results. Whether the visco-elastic behaviour can be accurately described, a new design strategy can be developed towards the final goal.

7. Conclusions

The research has regarded several aspects of the ambitious project of designing multistable structures for space applications such as packageable and morphing mirrors, antennas, solar arrays.

A first phase was devoted to the characterization of the glass fibre / epoxy composite, as great advantages with respect to metallic materials - in terms of stiffness-to-weight ratio and electromagnetic interference - were recognized.

Analytical models with increasing degrees of accuracy yet complexity have been used to describe the mechanical response of rectangular strips made of such material. Several problems such as visco-elasticity and stiffening due to artificially overconstrained boundary conditions forced additional tests and hypotheses.

On a higher level, hinges were manufactured and tested. Simple analytical models describe the complex structure as a series of strips subjected to pure bending or pure torsion; these models fail when the connections are weak, in which case a spurious displacement field is observed. The good prediction accuracy of numerical (FEM) models can help understanding the correct structural behaviour.

Visco-elasticity affects the overall structures badly. Techniques that try to mitigate this effect (such as manufacturing properly designed plates) have been employed. If the effect cannot be eliminated, additional effort should be put in creating design algorithms that are robust against this phenomenon.

8. Acknowledgments

I would like to thank ASI-CAIF for the immense support: the scholarship is an invaluable opportunity for personal and professional growth.

A sincere thanks goes to my supervisor, Prof. Sergio Pellegrino, for allowing me to join his research group and his magnificent laboratories.
I also want to thank Dr. Yang Li for the pleasant and rewarding time we spent working together.

References

[1] J N Reddy. *Mechanics of laminated composite plates and shells: theory and analysis*. 2003.

[2] Mark Schenk and Simon D. Guest. Geometry of Miura-folded metamaterials. *Proceedings of the National Academy of Sciences*, 2013.

[3] Hongbin Fang, Suyi Li, Huimin Ji, and K. W. Wang. Dynamics of a bistable Miura-origami structure. *Physical Review E*, 2017.

[4] F. Avilés, L. A. Carlsson, G. Browning, and K. Millay. Investigation of the sandwich plate twist test. *Experimental Mechanics*, 49(6):813–822, 2009.

[5] Raymond J. (Raymond Jefferson) Roark, Warren C. (Warren Clarence) Young, Richard G. (Richard Gordon) Budynas, and Ali M. Sadegh. *Roark's formulas for stress and strain.* 2012.

[6] Julio F. Davalos, Pizhong Qiao, Jialai Wang, Hani A. Salim, and Jeremy Schlussel. Shear moduli of structural composites from torsion tests. *Journal of Composite Materials*, 2002.

[7] H. Nikopour and A. P.S. Selvadurai. Torsion of a layered composite strip. *Composite Structures*, 2013.

[8] T.G. Nelson, R.J. Lang, S.P. Magleby, and L.L. Howell. Large-curvature deployable developable structures via lamina emergent arrays. In *Proceedings of the ASME Design Engineering Technical Conference*, 2015.